Supplementary Materials for

Effects of episodic slow slip on seismicity and stress near a subduction-zone megathrust

Authors: Saeko Kita[1*], Heidi Houston[2], Suguru Yabe[3], Sachiko Tanaka[4], Youichi Asano[4], Takuo Shibutani[5], Naoki Suda[6]

Affiliations:

[1] Building Research Institute, National Research and Development Agency, Tsukuba, Ibaraki, Japan

[2] University of Southern California, Los Angeles, California, USA

[3] National Institute of Advanced Industrial Science and Technology (AIST), Tsukuba, Ibaraki, Japan

[4] National Institute of Earth Science and Disaster Resilience (NIED), Tsukuba, Ibaraki, Japan

[5] DPRI, Kyoto University, Uji, Kyoto, Japan

[6] Hiroshima University, Higashi-Hiroshima, Hiroshima, Japan

* Currently at the Department of Earth and Planetary Science and Berkeley Seismolab, University of California, Berkeley, California, USA

Correspondence to: kita@kenken.go.jp

This PDF file includes:

Supplementary Text

Text S1

Detailed stress regime for interplane and lower-plane events

Figures 2i and 2j show the results of stress tensor inversions for interplane and lower-plane events using the focal mechanisms shown in Figs. S1e and S1f.

In the results for the interplane and lower-plane events, the difference in dip for the best fit σ1 before ETS and that after ETS times was more than 40 degrees (Figs. 2i and 2j and Table S1), and the 90% confidence limits for σ1 after the ETS are broadly distributed in the strike direction for σ1. Beneath northeastern Japan, the confidence levels for σ1 in the interplane and lower-plane events for the double seismic zone in the Pacific slab are larger than that in the upper-plane[1], so that the unstable trend of σ1 in the present study on stress inversions of the oceanic mantle events is reasonable.

Furthermore, we examined stress changes for interplane and lower-plane events beneath three regions: the updip of the ETS zone, the ETS zone, and the downdip of the ETS zone shown in Fig. S2 and Table S2. The stress change beneath the ETS zone (Figs. S2e through S2f and Table S2) is relatively small, as compared to those beneath the updip and downdip regions of the ETS zone (Figs. S2a, S2b, S2i, and S2j and Table S2). Although the number of events used in the inversion is insufficient, we can see a trend whereby stress changes in the interplane and lower-plane events after the ETS beneath the updip and downdip regions of the ETS zone. Geological and petrological studies indicated that geofluid migrates in the direction of σ2[2, 3, 4]. Since σ2 for the interplane and lower-plane events beneath the updip and downdip of the ETS zone is not the direction of the dip of the plate, the geofluid from the oceanic mantle beneath the updip and downdip of the ETS zone can migrate to the plate interface.

In summary, stress changes for the interplane and lower-plane events after the ETS times are found, but, similar to the results beneath the northeastern subduction zone, they are not clearly different from the characteristics of the unstable stress regime in the oceanic mantle[1]. Moreover, the distance from the plate interface to the oceanic mantle is larger than that from the interface to the oceanic crust, and the explanation of the time change in stress in the upper-plane events associated with the ETS times seems more reasonable.

Text S2

b-value change before and after ETS times in each region

Figure 3c in the main text shows the b-values versus the assumed lower limit of the analysis magnitude (Mc) for the combined 3 regions, demonstrating that b-values are higher before the occurrence of ETS. Supplementary Figures S3a through S3c show similar analyses for Regions A, B, and C, separately. Regions A and C are consistent with the overall pattern for the combined regions, whereas Region B does not show the change in b-values (red versus blue symbols). However, we note that the segmentation of tremor activity in Region B is less clear and several possible segment boundaries have been suggested, so that the association of in-slab seismicity and ETS timing may be less clear. Furthermore, Region B is relatively narrow. Thus, it seems clear that b-values of in-slab earthquakes beneath Kii Peninsula generally decrease after the occurrence of ETS.

Text S3

Detailed time change of seismicity and b-values in upper-plane and other events

As shown in Fig. 3d, the b-values of in-slab events evolve with time over the ETS cycle, generally peaking about 1.5 months before ETS. A peak in the b-values before the ETS times is also seen when in-slab events are divided into upper-plane seismicity and lower-plane and interplane seismicity (Figs. S4a and S4b). Furthermore, if upper-plane in-slab events are divided into those in the ETS zone and those updip of the ETS zone, a peak in b-values before the ETS times is also seen (Figs. S4c and S4d).

The occurrence times of in-slab events versus distance along the strike of the subducting slab is shown in Supplementary Fig. S5a and S5b. The seismicity of upper-plane events is distributed uniformly, whereas that of interplane and lower-plane events are mainly distributed in Regions B and C.

Text S4

Time change of stress ratio R

We also examined the time change of the stress ratio R for stress tensor inversions using entire in-slab events beneath the compiled regions (Regions A, B, and C). The time change of the stress ratio R relative to the ETS times is shown in Fig. S6. Figure S6 shows the R value before ETS times exceeds 0.5, whereas that after ETS times decreases and becomes less than 0.5, which means that the dominant stress field changed at ETS times.

Text S5

Stability of stress tensor inversions

In order to show variations in the σ1 direction, we also applied bootstrap resampling tests to input data for the stress tensor inversions shown in Supplementary Figs. S1a through S1d. Figure S7 shows the result of stress inversions using 200-time resampling data, in which the distributions of the strike and dip angles of σ1 for each stress tensor inversion are shown. Beneath the updip zone, the distribution of the dip and strike angles after ETS times is clearly different from that before ETS times, whereas the distribution after ETS times does not overlap that before ETS times beneath the ETS zone.

We also examined the time change of the stress axis of stress tensor inversions for upper-plane events using a 1.5-month time window beneath the compiled regions. The results beneath ETS and updip zones are shown, respectively, in Supplementary Figs. S8 and S9.

References (1-4):

1. Kita, S., Okada, T., Hasegawa, A., Nakajima, J., Matsuzawa, T., Existence of interplane earthquakes and neutral stress boundary between the upper and lower planes of the double seismic zone beneath Tohoku and Hokkaido, northeastern Japan. *Tectonophysics*, **496**(1), 68–82 (2010).

2. Ogawa, Y., Vrolijk, P., Control of internal structure and fluid-migration pathways within the Barbados Ridge decollement zone by strike-slip faulting: Evidence from coherence and three-dimensional seismic amplitude imaging: Discussion. *Geol. Soc. Am. Bull.* **118**, 253–254 (2006)

3. Sibson, R.H., Generation of pseudotachylyte by ancient seismic pumping. *Geophys. J. R. Astron. Soc.*, **43**, 775-789 (1975).

4. Otsubo, M., Miyakawa, A., Katayama, I., Okazaki, K., An inhomogeneous across-slab conduit controlled by intraslab stress heterogeneity in the Nankai subduction zone. *Scientific Reports*, **9**, 994 (2019).

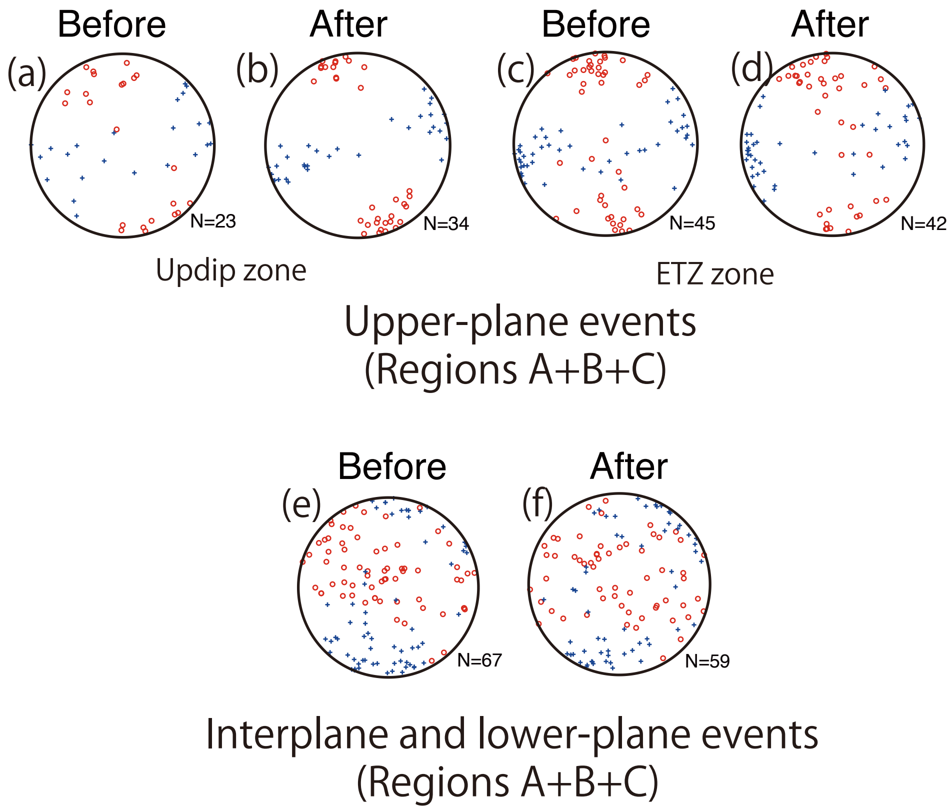

Fig. S1.
Input data of stress tensor inversions shown in Figures 2e through 2j. (a) and (b) Input data for stress tensor inversions (for upper-plane events beneath the updip of the ETS zone) shown in Figs. 2e and 2f, respectively. Lower hemisphere projections of the P- and T-axes, indicated by red circles and blue crosses, respectively, of focal mechanisms before and after ETS times. (c) and (d) Input data of stress tensor inversions for upper-plane events beneath the ETS zone shown in Figs. 2g and 2h. (e) and (f) Input data of stress tensor inversions for inter-plane and lower-plane events, respectively, shown in Figs. 2i and 2j.

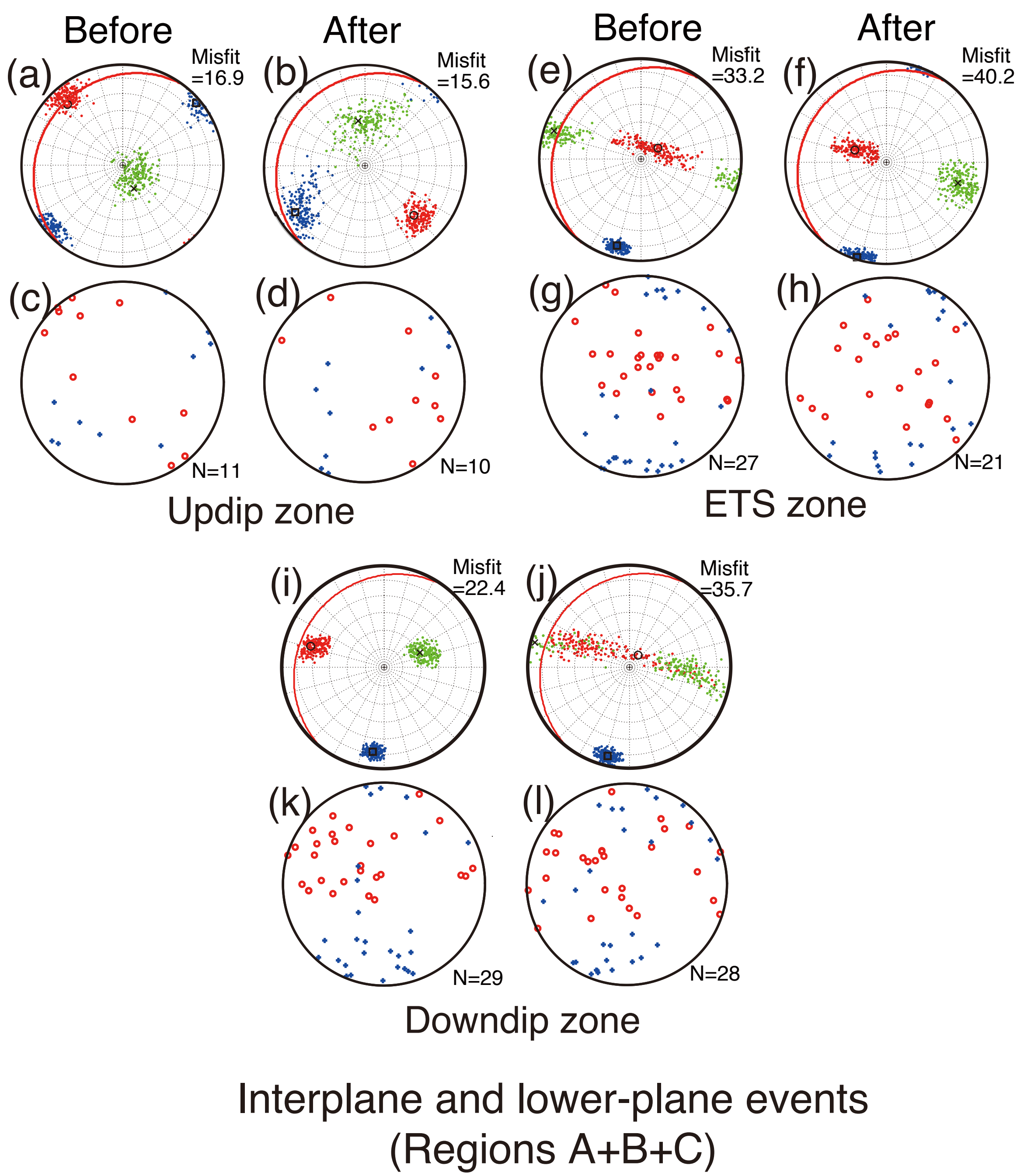

Fig. S2.

Results of stress tensor inversions for the interplane and lower-plane events (oceanic mantle events) and input data (focal mechanisms). (a) and (b) Results of the oceanic mantle events beneath the updip of the ETS zone before and after the ETS times. (c) and (d) Input data of (a) and (b), respectively. (e) and (f) Results of the inversions beneath the ETS zone. (g) and (h) Input data of (e) and (f), respectively. (i) and (j) Results beneath the downdip of the ETS zone. (k) and (l) Input data of (i) and (j), respectively.

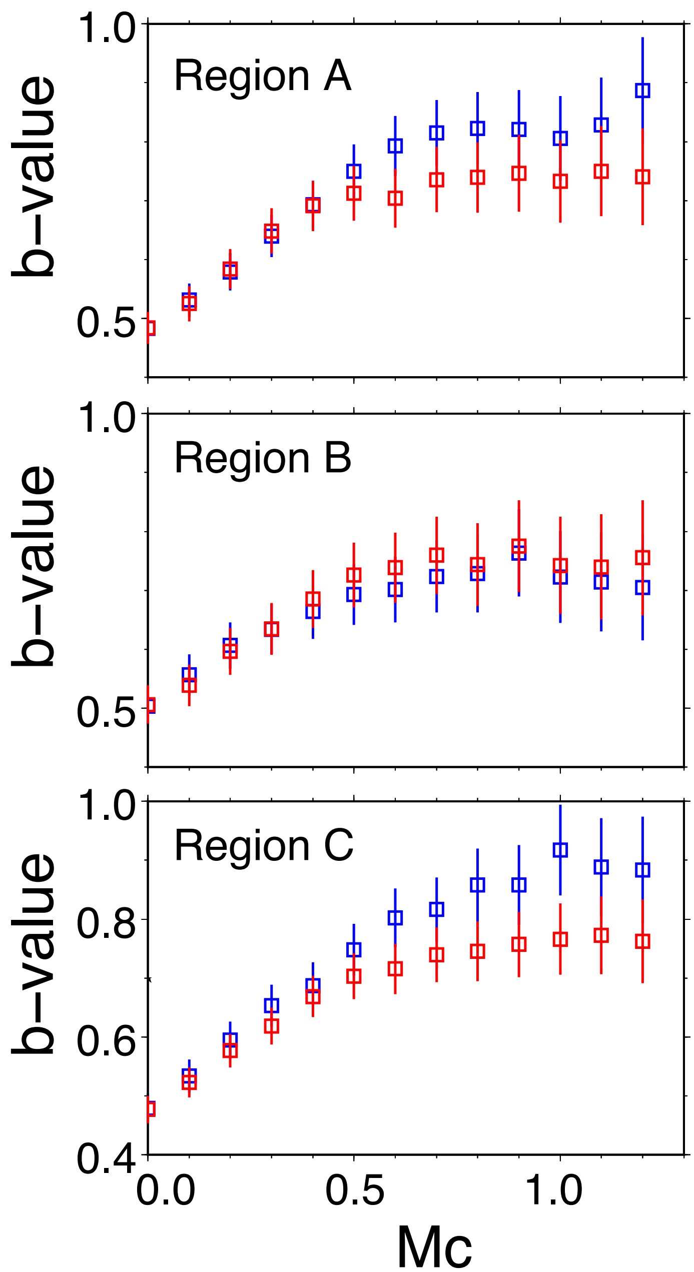

Fig. S3.

b-value versus lower limit of analysis magnitude (assumed Mc) for (a) Region A, (b) Region B, and (c) Region C. Red dots indicate b-values for events that occurred in two-month time windows before ETS times, and blue dots indicate b-values for events in two-month windows after ETS times.

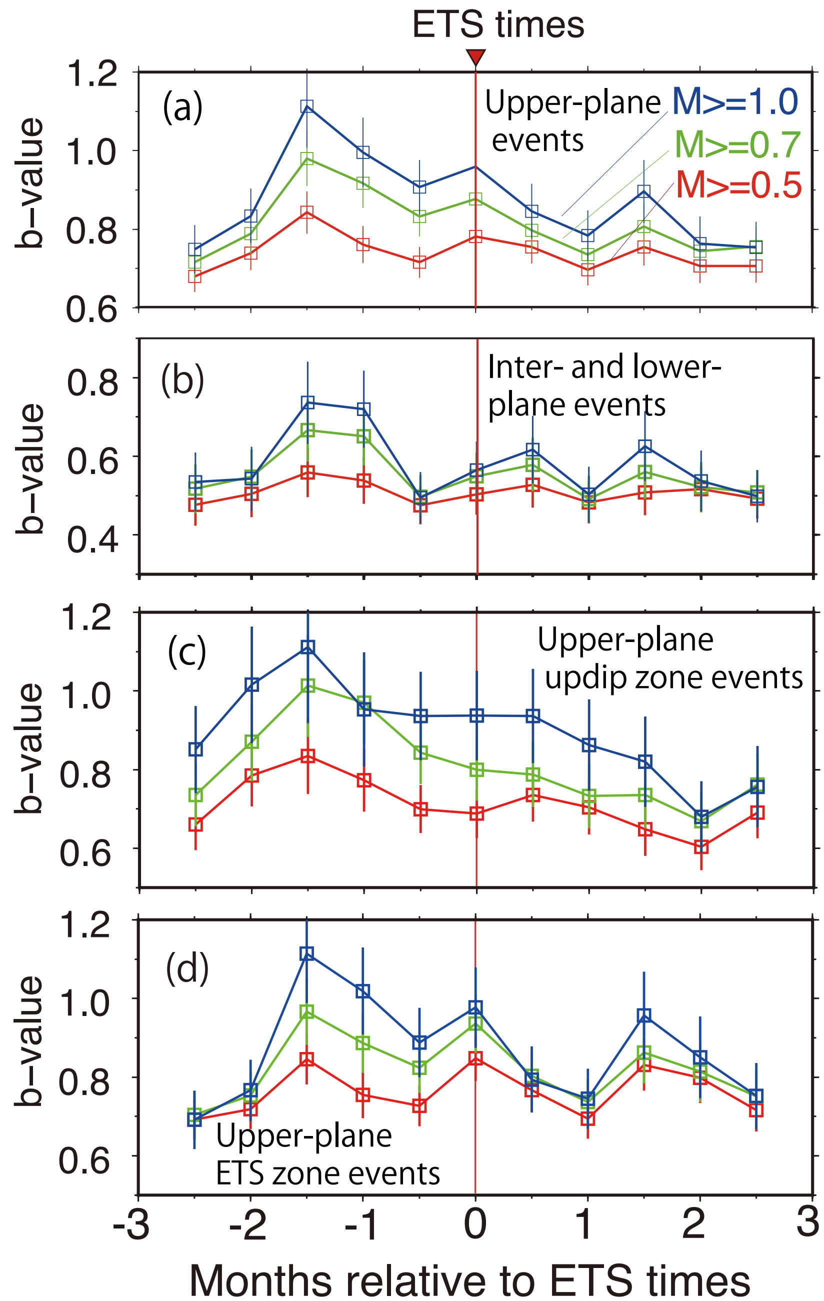

Fig. S4.
b-value time variation of (a) upper-plane events, (b) lower-plane and interplane events, (c) upper-plane events beneath the updip zone, and (d) upper-plane events beneath the ETS zone for the combined region using one-month moving windows. Red, green, and blue dots indicate the estimated b-values for Mc values of 0.5, 0.7 and 1.0, respectively.

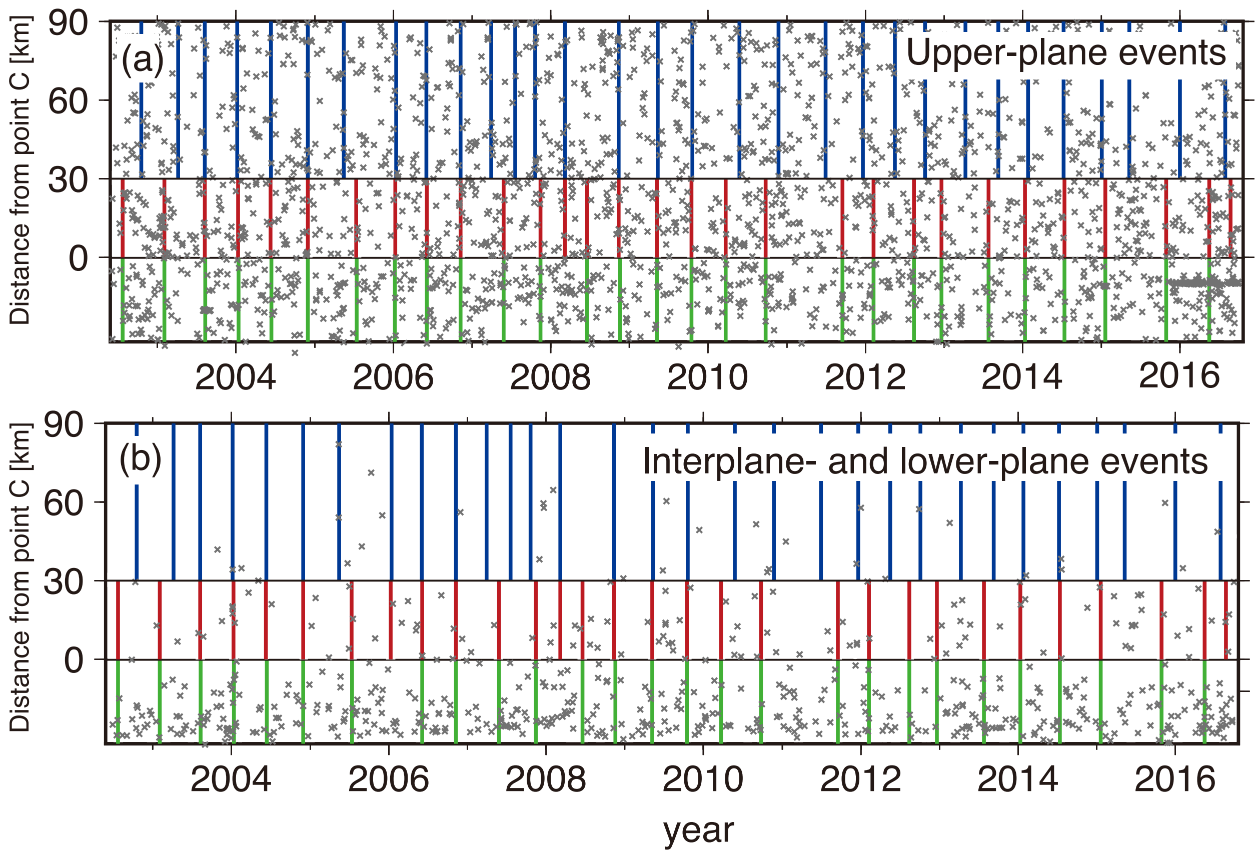

Fig. S5.
In-slab earthquake occurrence times versus distance along the strike of the subducting slab. Gray crosses indicate (a) upper-plane events and (b) lower-plane and interplane events. The division of regions is shown in Fig. 1a. The distance along the strike is measured from point C in Fig. 1a.

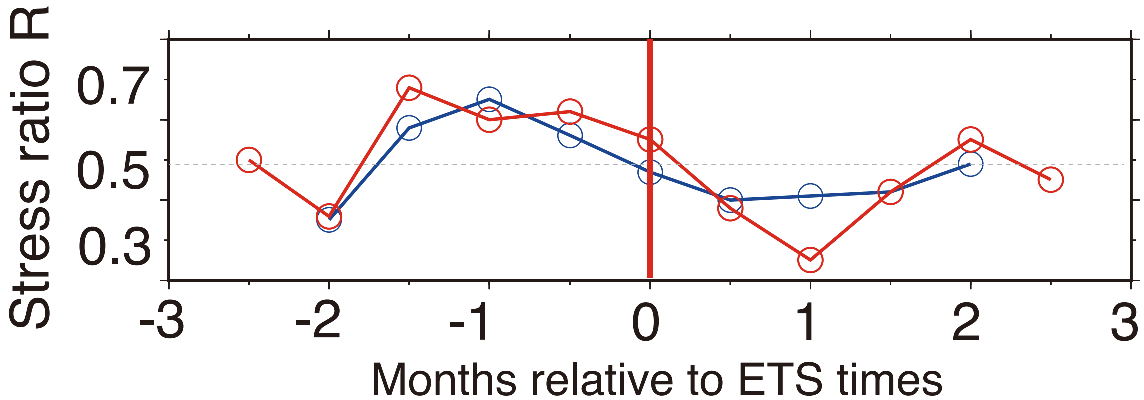

Fig. S6.

Stress ratio R time variation. R values for stress inversions of all in-slab events using one and two-month moving windows are indicated by red and blue dots, respectively. A value of R close to 0 indicates single-axis tension, whereas a value of R close to 1 indicates single-axis compression. Note that the time change of R in the present study indicates the dominant stress regime in the entire slab changes relative to the ETS times.

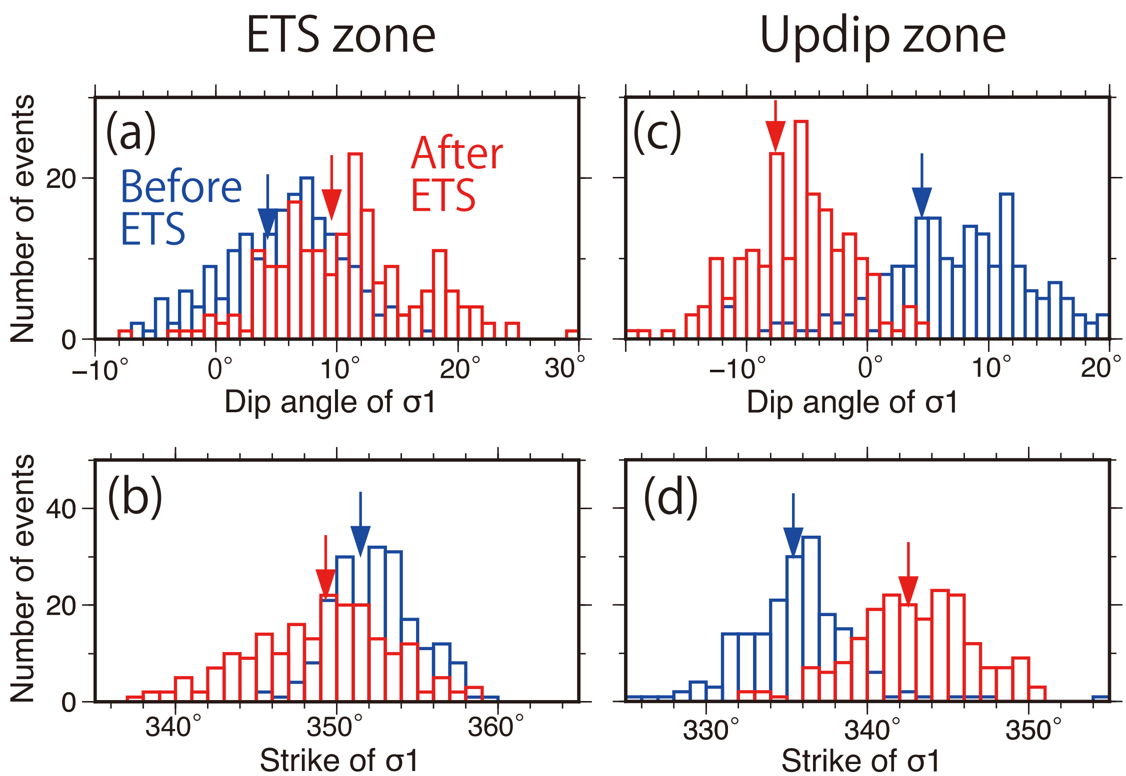

Fig. S7.

Results of 200 inversions of σ1 using bootstrap resampled focal mechanisms. Distributions of (a) dip and (b) strike angles of σ1 beneath the ETS zone. Blue and red columns, respectively, show the directions of σ1 of 200 inversions using events before and after ETS times. Blue and red arrows, respectively, show the directions of σ1 of the stress inversion using the original data set before and after ETS times. Distributions of (c) dip and (d) strike angles of σ1 beneath the updip zone.

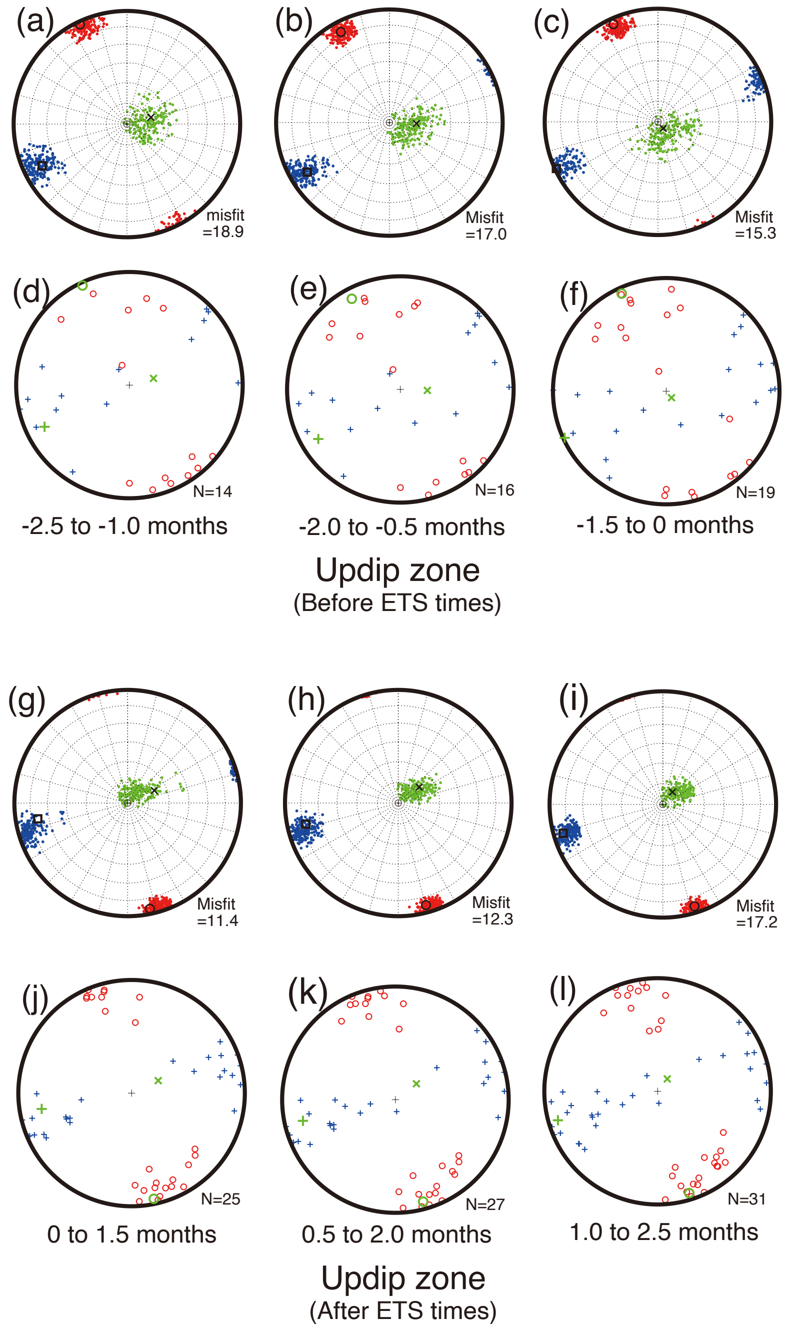

Fig. S8

Results of stress tensor inversions for the upper-plane events and input data (focal mechanisms) beneath the ETS zone using a 1.5-month time window. (a), (b) and (c) Results before the ETS times using the input data of (d), (e) and (f), respectively. (g), (h) and (i) Results before the ETS times using the input data of (j), (k) and (l), respectively.

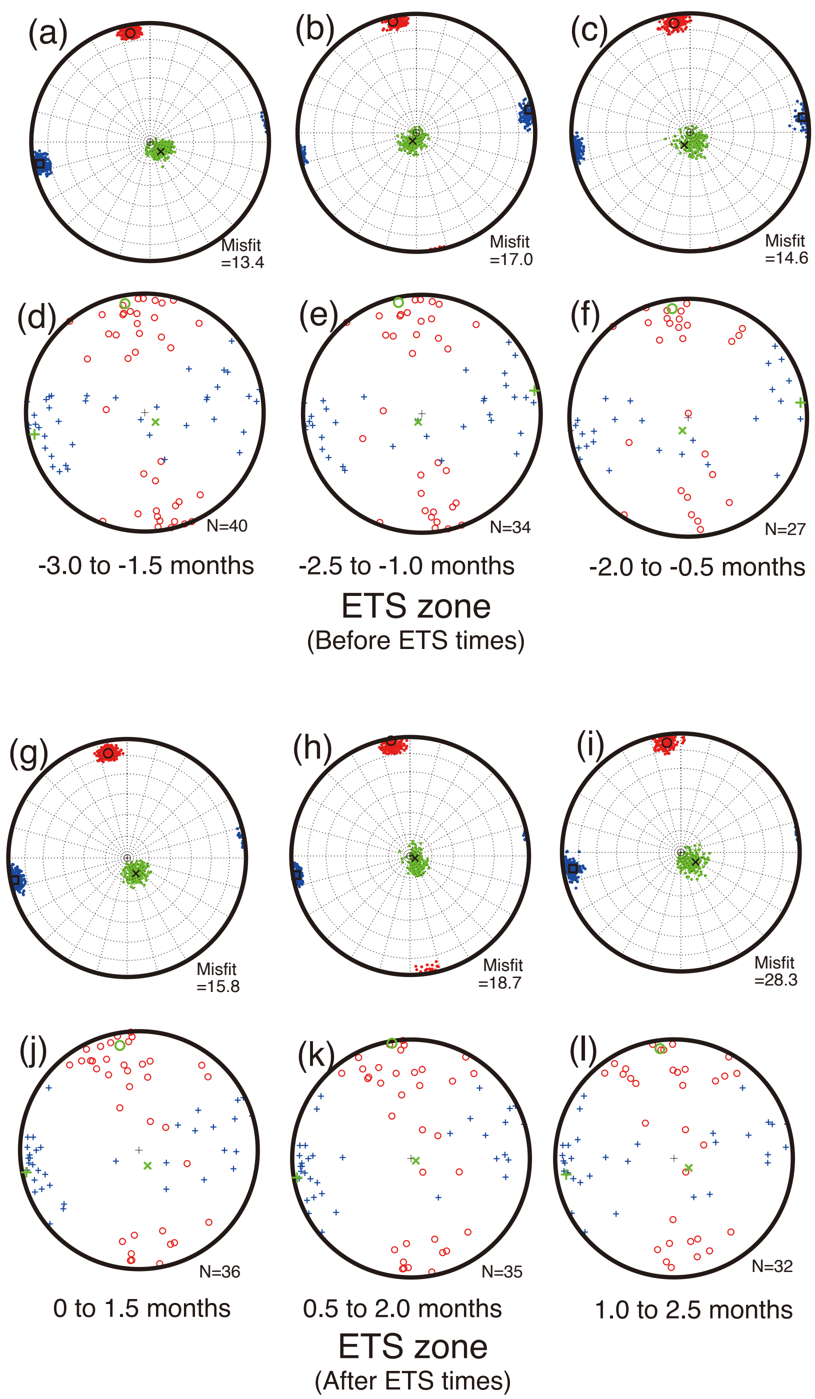

Fig. S9

Results of stress tensor inversions for the upper-plane events and input data (focal mechanisms) beneath the updip of the ETS zone using a 1.5-month time window. (a), (b) and (c) Results before the ETS times using the input data of (d), (e) and (f), respectively. (g), (h) and (i) Results before the ETS times using the input data of (j), (k) and (l), respectively.

Table S1.

Results of stress tensor inversions: Upper-plane events beneath the ETS zone of the three regions (Region A+B+C), upper-plane events beneath the updip of the ETS zone of the three regions, and oceanic mantle events (interplane and lower-plane events) beneath the three regions. σ1: maximum compressive stress, σ2: intermediate principal stress, σ3: minimum compressive stress, Misfit: average misfit angle. The contents of Table S1 plotted on the lower hemisphere are also shown in Figs. 2e through 2j.

Event name	Sigma 1				Sigma 2				Sigma 3				Misfit		Num. of events		Stress ratio R	
	Before		After		Before		After		Before		After		Before	After	Before	After	Before	After
	strike	dip	strike	dip	strike	dip	strike	dip	strike	dip	strike	dip						
Updip zone (Upper-plane)	335.5	5.9	163.3	7.03	87.5	74.5	35.9	78.5	244	14.2	254.5	9.0	20.1	12.3	23	34	0.83	0.88
ETS zone (Upper-plane)	351.9	4.6	349.2	9.3	187.8	85.2	145.1	79.8	82.0	1.3	258.5	4.1	15.3	17.4	45	42	0.71	0.67
Oceanic mantle, entire (inter-plane and lower-plane)	299.1	38.1	355.2	80.3	92.2	48.7	110.4	4.17	198.2	13.6	201.1	8.7	32.9	44.8	67	59	0.31	0.09

Table S2.

Results of stress tensor inversions: Interplane and lower-plane events (oceanic mantle events) beneath the ETS zone, updip of the ETS zone, and downdip of the ETS zone of the three regions. The contents of Table S2 plotted on the lower hemisphere are also shown in Figs. S2a, S2b, S2e, S2f, S2i, and S2j.

Event name	Sigma 1				Sigma 2				Sigma 3				Misfit		Num. of events		Stress ratio R	
	Before		After		Before		After		Before		After		Before	After	Before	After	Before	After
	strike	dip	strike	dip	strike	dip	strike	dip	strike	dip	strike	dip						
Oceanic mantle, updip zone	317.8	20.1	135.3	31.4	154.5	69.1	351.4	52.9	49.8	5.5	351.4	52.9	15.6	26.5	11	10	0.64	0.91
Oceanic mantle, ETS zone	57.3	73.8	291.3	62.7	287.9	10.5	106.2	27.3	195.6	12.3	197.2	2.1	33.2	40.2	27	21	0.25	0.53
Oceanic mantle, downdip zone	286.0	25.5	35.3	78.1	67.7	58.7	284.7	4.2	187.7	16.9	193.8	11.1	22.4	35.7	29	28	0.51	0.13

Table S3.
Results of stress tensor inversions: Upper-plane events beneath the ETS zone of the three regions using a 1.5-month time window. The contents of Table S3 plotted on the lower hemisphere are also shown in Figs. S8a through S8c and S8g through S8i.

	Sigma 1		Sigma 2		Sigma 3				
Event name	strike	dip	strike	dip	strike	dip	Misfit	Num. of events	Stress ratio R
-2.5 to -1.0 months	334.8	3.1	74.3	72.0	243.8	17.7	18.9	34.0	0.68
-2.0 to -0.5 months	331.9	10.1	92.0	70.6	238.9	16.5	17.0	27.0	0.84
-1.5 to 0.0 months	335.5	5.8	141.1	84.0	245.3	1.5	15.3	39.0	0.82
0 to 1.5 months	348.1	-5.1	64.9	68.8	260.0	20.5	11.4	36.0	0.87
0.5 to 2.0 months	343.8	-6.6	52.9	72.1	255.8	16.6	12.4	35.0	0.93
1.0 to 2.5 months	342.7	-6.5	37.9	78.7	253.8	9.2	17.2	32.0	0.72

Table S4.
Results of stress tensor inversions: Upper-plane events beneath the updip of the ETS zone of the three regions using a 1.5-month time window. The contents of Table S4 plotted on the lower hemisphere are also shown in Figs. S9a through S9c and S9g through S9i.

	Sigma 1		Sigma 2		Sigma 3				
Event name	strike	dip	strike	dip	strike	dip	Misfit	Num. of events	Stress ratio R
-2.5 to -1.0 months	348.1	4.9	204.7	83.9	78.4	3.6	16.7	34	0.72
-2.0 to -0.5 months	351.6	8.1	204.2	80.4	82.4	5.1	14.5	27	0.71
-1.5 to 0.0 months	353.2	1.7	241	85.5	83.4	4.1	17.7	39	0.70
0 to 1.5 months	349.7	11.5	150.6	77.8	258.9	3.9	15.8	36	0.69
0.5 to 2.0 months	350.6	2.0	114.2	86.4	260.5	3.0	18.7	35	0.48
1.0 to 2.5 months	352.7	7.8	122.8	78.0	261.5	9.1	28.3	32	0.66